Short-T_R, Spoiled, Gradient Echo Imaging

OVERVIEW

The simplest gradient echo sequence has a dephasing gradient and a rephasing gradient to form an echo in the read direction. If 256 phase encoding steps are required, then the sequence has 256 RF pulses with one unique phase encoding gradient and two gradients in the read direction per RF excitation (excluding slice select gradients and spoiler gradients).

When a spin system is repeatedly disturbed by a fast repetition of RF pulses, the regrowth of the longitudinal magnetization is limited due to the finite repetition time T_R in the read direction. After many RF pulses, the transverse magnetization approaches a steady-state value which is smaller than the thermal equilibrium value. The spin system takes a finite number of RF pulses (n_α) before this steady-state is reached (to within some tolerance at least) in a time ($n_\alpha T_R$) that depends on both the T_1 of the tissue and the flip angle of the RF pulse. This time is usually on the order of several T_1.

Sequences utilizing a steady-state approach can be broadly classified as steady-state incoherent (SSI) and steady-state coherent (SSC) sequences. The main difference between the two lies in whether or not the transverse magnetization is forced to zero or allowed to go naturally to steady-state between successive RF pulses. As the nomenclature suggests, the SSI sequences are based on the elimination, or the "spoiling," of any remnant transverse magnetization prior to the occurrence of each new RF pulse (see Fig. B5.1.1). This unit discusses the SSI sequences in detail.

Figure B5.1.2, panel A, illustrates the magnetization in one RF pulse cycle. The steady state magnetization M_{ze} along z is tipped by the RF pulse in the $(n + 1)$st RF cycle. Due to the T_1 relaxation, the longitudinal magnetization grows back to M_{ze} at the end of that

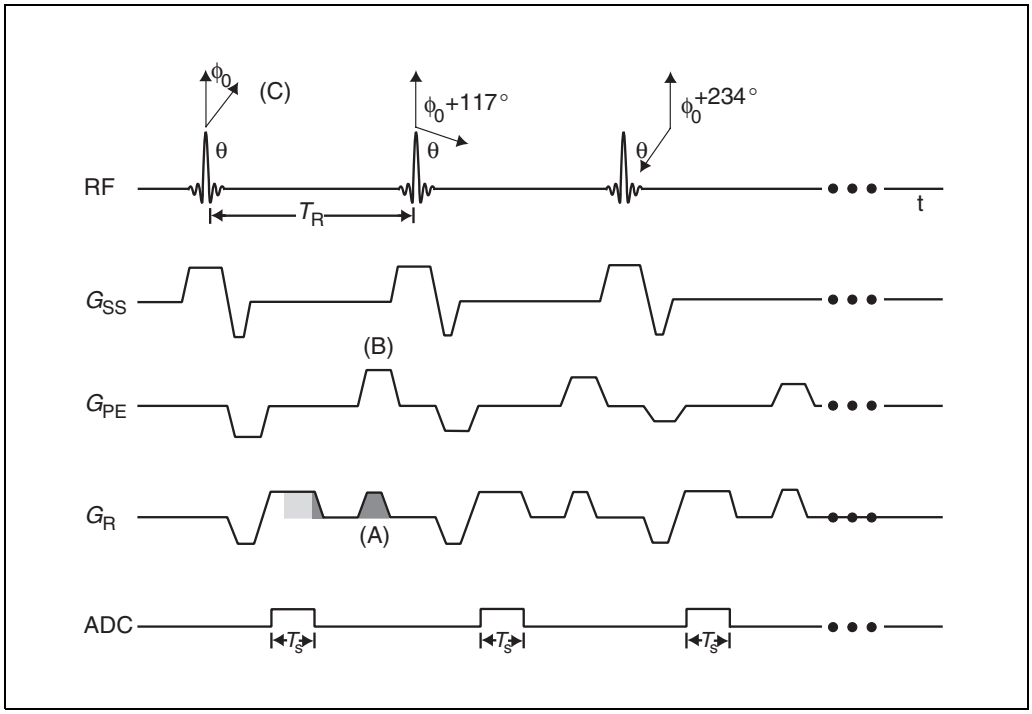

Figure B5.1.1 An RF spoiled implementation of an SSI imaging sequence. Note that the areas under the read gradient during the second half of sampling and the rest of the read gradient waveform (shown with denser shading) are the same.

Contributed by Yu-Chung Norman Cheng and E. Mark Haacke

Current Protocols in Magnetic Resonance Imaging (2001) B5.1.1-B5.1.16

cycle. Thus, every RF cycle after that cycle will produce the same transverse magnetization for a given tissue. The MR signal as a function of flip angle θ at the echo time is then given by:

$$\hat{\rho}(\theta) = \rho_0 \sin\theta \frac{1 - e^{-T_R/T_1}}{1 - e^{-T_R/T_1}\cos\theta} e^{-T_E/T_2^*} \quad \textbf{(B5.1.1)}$$

where ρ_0 is the original spin density of the tissue.

This transverse magnetization has a maximum as a function of the flip angle. This can be understood as follows. When the flip angle is close to zero, so is the transverse magnetization, since little transverse magnetization is created. On the other hand, when the flip angle is close to 90°, after many RF pulses, the transverse magnetization again approaches a small number since the longitudinal magnetization does not have enough time to grow between RF pulses. Thus, for flip angles between 0° and 90°, there must be an optimal flip angle which gives the maximum signal. This flip angle is called the Ernst angle, and is given by:

$$\theta_E \equiv \cos^{-1}\left(e^{-T_R/T_1}\right) \quad \textbf{(B5.1.2)}$$

When T_R is much smaller than T_1, the Ernst angle can be approximated as:

$$\theta_E \simeq \sqrt{\frac{2T_R}{T_1}} \quad \textbf{(B5.1.3)}$$

Note carefully the square root dependence of the Ernst angle on T_R and T_1. Figure B5.1.3 shows the simulations of signals of white matter and gray matter versus the flip angle and Figure B5.1.4 shows images of the brain scanned at three different flip angles.

For a given flip angle, it always takes a certain number of RF pulse cycles to reach the steady state in an SSI sequence. Figure B5.1.5 demonstrates this concept for four different tissues; however, it usually takes more than 30 pulses to reach the steady state depending on how close the desired approach is to the steady state magnetization. There are some cases where only a small number of consecutive RF pulses are applied. For example, this is usually found in cardiac imaging when segmented *k*-space is used and only a small number of phase encoding or partition encoding steps are applied per cardiac cycle. This transient sequence may create artifacts in 2-D (two-dimensional) or segmented 3-D (three-dimensional) imaging because the signal changes for every RF pulse. To avoid this difficulty one could use a variable flip angle in an attempt to maintain a constant transverse magnetization after each RF pulse. Figure B5.1.6 shows the simulation of the flip angle against the RF pulse number. Figure B5.1.7 compares two images where one was obtained by using a constant flip angle and the other by changing the flip angle from pulse to pulse to obtain a constant transverse magnetization. One can see the former one (Fig. B5.1.7, panel A) has more ringing than the latter because of the filter effect of the transverse magnetization not being constant from pulse to pulse.

Figures B5.1.8 and B5.1.9 show a multislice 2-D gradient echo and a double echo gradient echo sequence, respectively. These represent two different structures of a gradient echo sequence. Although it is possible that a multislice 2-D sequence due to its long T_R can have a higher MR signal than the signal from a short T_R 3-D sequence, any 2-D sequence will suffer from the effects of a non-boxcar slice profile; however, this is not a problem

in 3-D sequences. Clinically the SSI sequence is often used for 3-D T_1-weighted data in the brain, breathhold T_1 scans in the body and for MR angiography studies.

TECHNICAL DISCUSSION

This section presents detailed derivations of expressions for the steady-state magnetization components and their approach to steady-state incoherent equilibrium.

General Concept

Before an expression for the signal in the spoiled steady-state is obtained, it is worthwhile to see how the signal reaches a steady-state from its initial thermal equilibrium value. For a spin system initially at thermal equilibrium, the longitudinal magnetization is M_0. Let this spin system be acted on by a series of identical RF pulses of flip angle θ. After the first RF pulse, the longitudinal magnetization is given by:

$$M_z\left(0^+\right) = M_0 \cos\theta \qquad \textbf{(B5.1.4)}$$

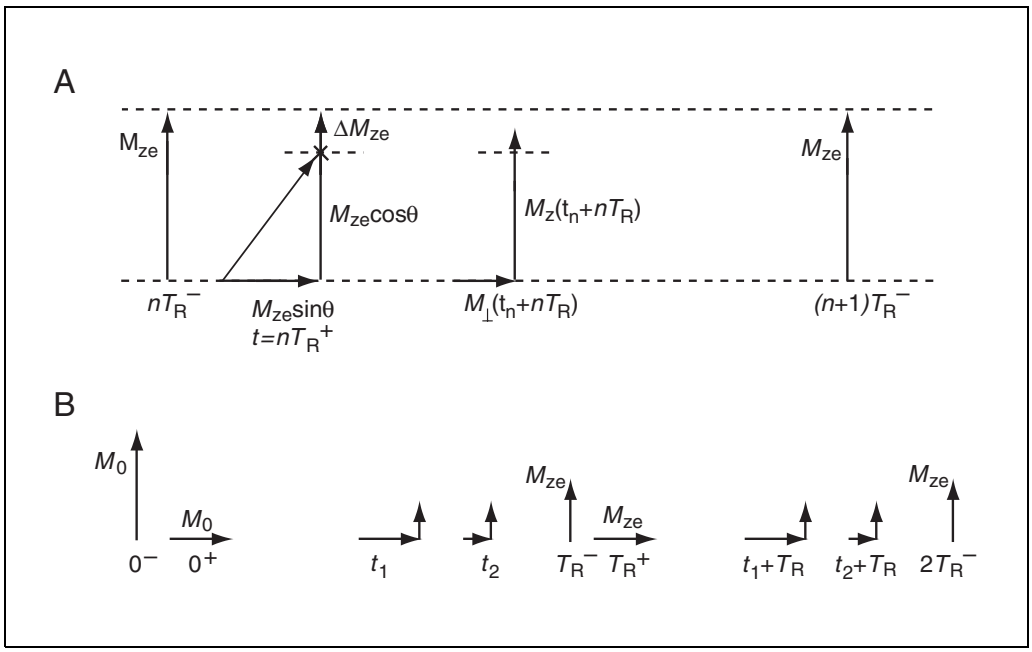

Figure B5.1.2 Evolution of the magnetization components at successive RF pulses (**A**) for an arbitrary flip angle θ and one steady-state RF cycle, and (**B**) for θ = π/2 and the first two RF pulses. The evolution in (A) begins at time $t = nT_R^-$ where only the steady-state magnetization M_{ze} is available. The application of a θ RF pulse at $t = nT_R$ creates a new transverse magnetization component M_{ze} sinθ while leaving behind longitudinal magnetization M_{ze} cosθ. The difference between the longitudinal magnetization before and after the RF pulse is represented by ΔM_{ze}. Between the (n + 1) and the (n + 2) RF pulses, the longitudinal magnetization starts regrowing towards M_0 by T_1 relaxation and the transverse component starts decaying towards zero due to T_2 relaxation. This is depicted by the components $M_z(t_n + nT_R)$ (lengthened) and $M_\perp(t_n + nT_R)$ (shortened in length). The evolution in (B) shows that, when θ = π/2, it takes only two RF pulses for the magnetization to reach steady-state. This occurs because each 90°-pulse tips all longitudinal magnetization, and it recovers to the same value $M_0(1 - e^{-T_R/T_1})$ during each subsequent period. For the first RF pulse alone, the initial magnetization is M_0; hence it takes two RF pulses to reach steady-state.

and the transverse magnetization by:

$$M_{\perp}\left(0^{+}\right) = M_0 \sin\theta \qquad \textbf{(B5.1.5)}$$

Between the first and second RF pulses, the longitudinal magnetization grows from the initial value $M_z(0^+)$ toward M_0 according to the Bloch equations. The longitudinal component has not necessarily reached its thermal equilibrium value by the time of the second RF pulse. At the same time, suppose that the transverse magnetization has been destroyed by some spoiling mechanisms. At the end of the first repetition cycle, $M_z(T_R^-)$ is again transformed into longitudinal and transverse components by the second RF pulse, and this process continues.

After a sufficient number of cycles, the process reaches a steady-state defined by a recurrence of the same magnetization values and identical behavior in each RF cycle. This process is illustrated for one cycle in the steady-state for an arbitrary θ-pulse in Figure B5.1.2, panel A. In this steady-state limit, the magnetization is periodic with period T_R. The steady-state values are reached when the loss in longitudinal magnetization due to its tipping by the RF pulse is exactly counterbalanced by its growth due to T_1 recovery during the inter-pulse period. In general, there is an initial transient behavior before the magnetization settles into this periodicity. Notice from Figure B5.1.2, panel B that the magnetization reaches steady-state after the second pulse when $\theta = \pi/2$. In general, the number of pulses required to reach steady-state is a function of the flip angle and T_R. The process of achieving steady-state and the dependence on the number of pulses required to reach steady-state are described below.

Expression for the Steady-State Incoherent (SSI) Signal

We begin with the simplest concepts that describe short-T_R steady-state incoherent imaging. These imaging methods are often referred to as FLASH (Fast Low Angle Shot) or spoiled GRASS (Gradient Refocused Acquisition in the Steady-State). In the nomenclature introduced here, they are referred to as short-T_R SSI gradient echo methods. Consider a gradient echo sequence where $T_R >> T_2$. This is the situation where $M_{\perp}(nT_R^-) = 0$, where $t = nT_R$ is the instant of occurrence of the $(n + 1)^{st}$ RF pulse. This is a naturally spoiled sequence where all transverse magnetization is essentially zero before the next RF pulse. We wish to find a solution to the steady-state longitudinal magnetization for a given isochromat, for given values of T_1, T_2, T_R and flip angle θ. (When the isochromat is replaced by a voxel, T_2 must be replaced by T_2^* for gradient echo imaging.) The following analysis is valid for an isochromat of spins where there are no T_2^* effects.

The transverse magnetization decays during each evolution period:

$$M_{\perp}\left(t_n\right) = M_{\perp}\left(0^{+}\right)e^{-t_n/T_2} \qquad 0 < t_n < T_R \qquad \textbf{(B5.1.6)}$$

where $M_{\perp}(0^+)$ is a shorthand notation for $M_{\perp}(t_n = 0^+)$. The total time from the first pulse is t, and the relative time within each cycle is defined as:

$$t_n \equiv t - nT_R \qquad \textbf{(B5.1.7)}$$

The regrowth of longitudinal magnetization during this period is:

$$M_z\left(t_n\right) = M_0\left(1 - e^{-t_n/T_1}\right) + M_z\left(0^{-}\right)e^{-t_n/T_1} \qquad \textbf{(B5.1.8)}$$

where $M_z(0^-)$ is shorthand notation for $M_z(t_n = 0^-)$. Equation B5.1.6 and Equation B5.1.8 can be rewritten by reintroducing the total time:

$$M_\perp\left((n+1)T_R^-\right) = M_\perp\left(nT_R^+\right)E_2 = M_z\left(nT_R^-\right)\sin\theta E_2 \quad \textbf{(B5.1.9)}$$

which goes to zero as E_2 goes to zero. Under these circumstances:

$$M_z\left((n+1)T_R^-\right) = M_z\left(nT_R^-\right)\cos\theta E_1 + M_0\left(1-E_1\right) \quad \textbf{(B5.1.10)}$$

where E_1 and E_2 are defined by

$$E_1 \equiv e^{-T_R/T_1} \quad \textbf{(B5.1.11)}$$

and

$$E_2 \equiv e^{-T_R/T_2} \quad \textbf{(B5.1.12)}$$

for convenience.

The attainment of the steady-state by the time of the *N*th pulse implies that the value of M_z just prior to each subsequent RF pulse is unchanged from cycle to cycle. Define the steady-state equilibrium value of M_z to be M_{ze} so that:

$$M_z\left(mT_R^-\right) = M_{ze} \qquad m \geq N \quad \textbf{(B5.1.13)}$$

From Equation B5.1.10 and Equation B5.1.13, M_{ze} must satisfy:

$$M_{ze} = M_{ze}E_1\cos\theta + M_0\left(1-E_1\right) \quad \textbf{(B5.1.14)}$$

This yields the steady-state or equilibrium value:

$$M_{ze} = \frac{M_0\left(1-E_1\right)}{\left(1-E_1\cos\theta\right)} \quad \textbf{(B5.1.15)}$$

Plugging in this result into Equation B5.1.6 gives:

$$M_\perp\left(\theta, t_n\right) = M_{ze}\sin\theta e^{-t_n/T_2} = \frac{M_0\sin\theta\left(1-E_1\right)}{\left(1-E_1\cos\theta\right)}e^{-t_n/T_2} \qquad 0 < t_n < T_R \quad \textbf{(B5.1.16)}$$

under steady-state equilibrium.

The only changes in Equation B5.1.16 needed to represent the steady-state signal from a voxel containing several isochromats are the replacements of M_0 by ρ_0 (the voxel spin density) and T_2 by T_2^*. Hence,

$$\hat{\rho}(\theta, T_E) = \rho_0 \sin\theta \frac{(1 - E_1)}{(1 - E_1 \cos\theta)} e^{-T_E/T_2^*} \quad \textbf{(B5.1.17)}$$

Figure B5.1.3 shows the general behavior of $\hat{\rho}$ as a function of θ for both white matter (WM) and gray matter (GM). The maximum signal occurs for an intermediate angle (less than $\pi/2$) defined as the Ernst angle θ_E:

$$\theta_E \equiv \cos^{-1} E_1 \quad \textbf{(B5.1.18)}$$

When $T_R << T_1$:

$$\theta_E \simeq \sqrt{\frac{2T_R}{T_1}} \quad \textbf{(B5.1.19)}$$

Note that Equation B5.1.17 vanishes at $\theta = 0$ due to the $\sin\theta$ factor (the E_1 dependence cancels out in this limit). But the E_1 dependence in the numerator is not canceled for larger angles, and yields an approximate suppression factor T_R/T_1 for small T_R. In fact, when $\theta = 90°$, the signal is directly proportional to T_R/T_1, as illustrated in Figure B5.1.3B.

An interesting feature of the SSI sequence is that it is possible to obtain spin-density weighting even for small T_R values ($T_R << T_1$). In the low flip angle, short-T_R limit, the SSI signal will be seen to be linearly proportional to ρ_0 and θ, and independent of T_1 and T_2. The linear relationship to flip angle is shown in the plots of Figure B5.1.3A. Further, note that the slope is lower for WM which has a lower relative spin density as shown in Table B5.1.1.

At low flip angles, $\cos\theta \cong 1$ and $\sin\theta \cong \theta$, and the expression for $\hat{\rho}$ can be approximated by $\rho_0\theta$. From Figure B5.1.3A, one can see that this approximation is good when θ is less than ~5° for WM and GM.

Other features of practical interest are the zero crossing of the SSI signal for all tissues when the flip angle equals 180° and the achievement of T_1-weighted contrast (suppression of long T_1 tissues) that occurs past the Ernst angle. This latter feature is seen in Figure B5.1.3B where WM has a higher signal than GM (GM has a longer T_1 value; see Table B5.1.1) for flip angles greater than $\theta_{E,WM}$. The contrast stays approximately constant past the Ernst angle, a feature which is utilized to obtain T_1-weighted contrast at flip angles much lower than 90°. The important features of SSI signal behavior are demonstrated in the images shown in Figure B5.1.4, for T_R = 20 msec, $\theta_{E,CSF} \cong 5°$, $\theta_{E,GM} \cong 12°$, $\theta_{E,WM} \cong 15°$ and $\theta_{E,fat} \cong 23°$. With these conditions, it is expected that CSF will have the highest signal (highest ρ_0) in a $\theta = 2°$ image, while WM will have the lowest signal as seen in Figure B5.1.4A. WM and GM have a signal cross-over for ~$\theta = 10°$, yielding no WM/GM contrast while CSF is T_1-weighted, leading to a heavy suppression of its signal (Fig. B5.1.4B). For $\theta = 20°$, good T_1-weighted contrast is obtained between GM and WM. CSF is suppressed further and fat now has the highest signal (Fig. B5.1.4C). These findings are further illustrated in the plots of the voxel signal as a function of flip angle for these four tissues in Figure B5.1.4D.

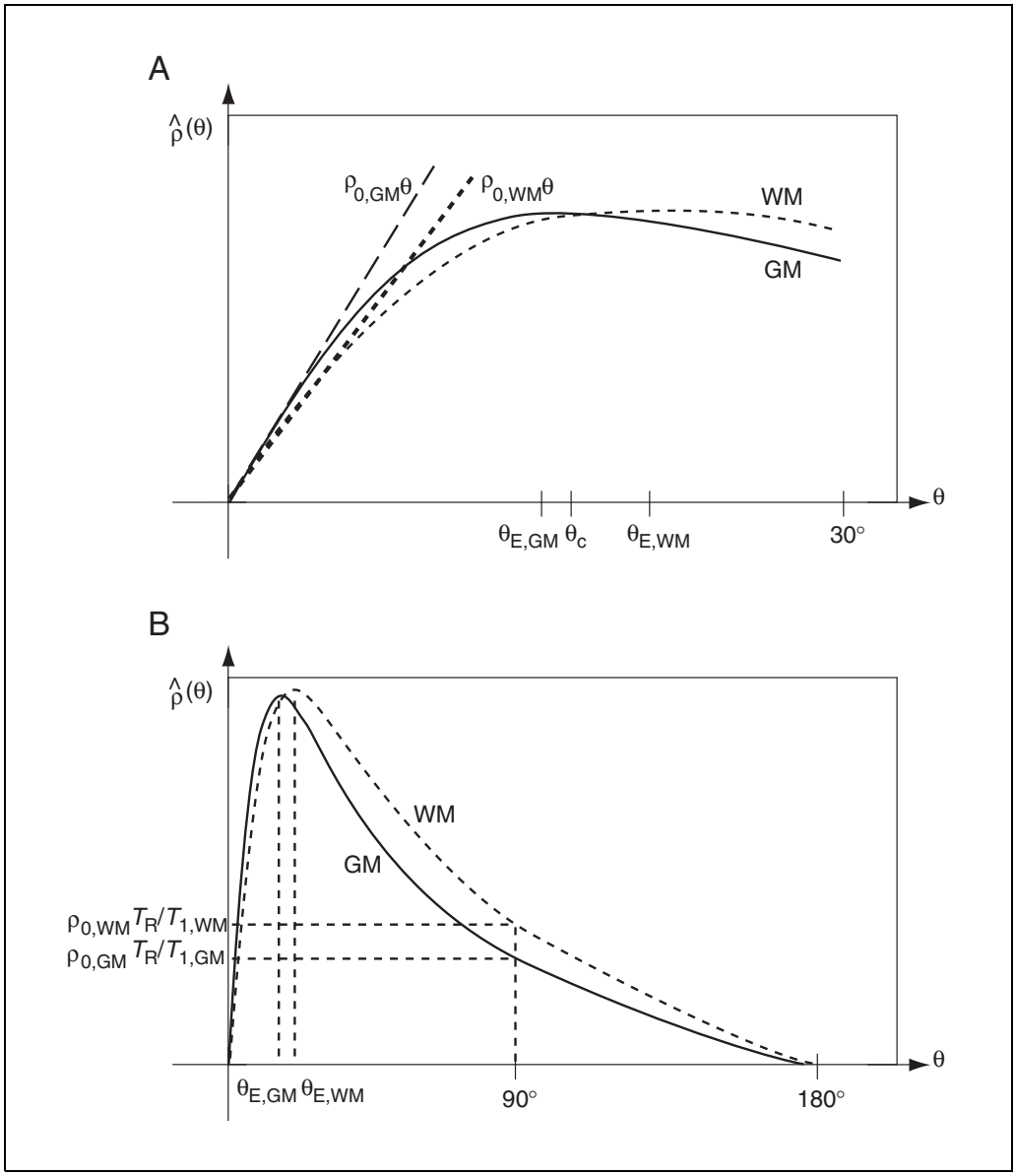

Figure B5.1.3 Comparison of the SSI signal behavior of gray matter (GM) and white matter (WM) for the representative values of T_R = 40 msec and T_E = 0 msec. Parameters are given in Table B5.1.1. (**A**) Small flip angle signal behavior. The angles $\theta_{E,GM}$ and $\theta_{E,WM}$ denote the Ernst angles of GM and WM, respectively, and θ_c denotes the flip angle at which the two curves cross each other (i.e., the cross-over point). (**B**) SSI signal behavior for the range $0 \leq \theta \leq \pi$.

Table B5.1.1 Estimated NMR Properties of Cerebrospinal Fluid (CSF), WM, GM and Fatty Tissue at 1.5 T

Tissue	ρ_0[a]	T_1 (msec)	T_2 (msec)
CSF	1.0	4500	2200
WM	0.65	600	80
GM	0.8	950	100
Fatty tissue	0.9	250	60

[a]Here, ρ_0 is the spin density relative to CSF.

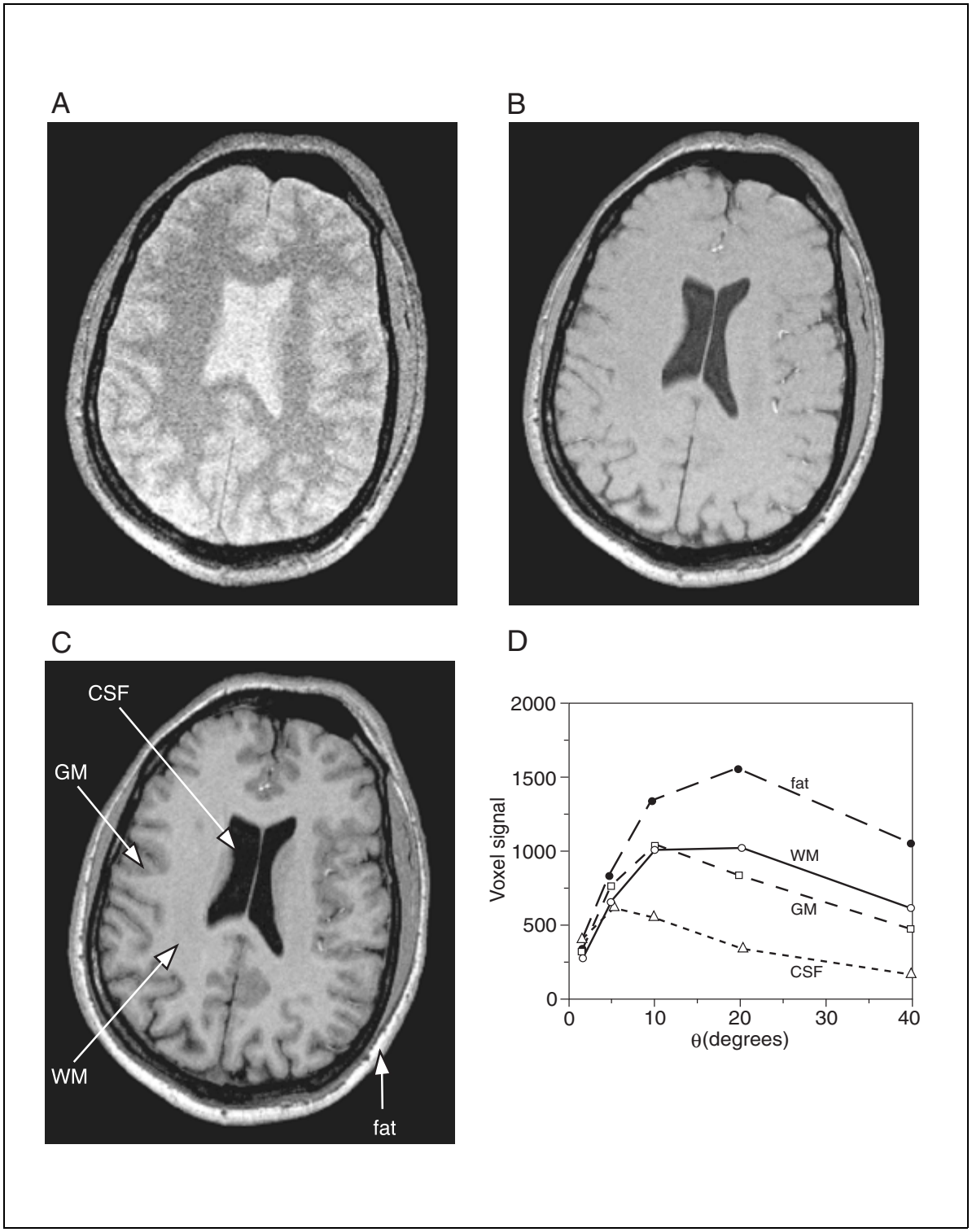

Figure B5.1.4 Images obtained with a 3-D SSI sequence at different flip angles using a 20 msec T_R. (**A**) Image for $\theta = 2°$ is spin density-weighted: CSF is the brightest, GM is intermediate and WM has the lowest signal. (**B**) Image for $\theta = 10°$ shows the effect due to the cross-over between the GM and WM signal curves; note the absence of GM-WM contrast. (**C**) Image for $\theta = 20°$ is T_1-weighted; the appearance is reversed from that of the spin density-weighted image. (**D**) The measured image signal $\hat{\rho}$ in arbitrary units as a function of flip angle θ from this data set. Imaging parameters: (a) T_R/T_E = 20 msec/4.7 msec, T_s = 10.24 msec, $\Delta x \times \Delta y \times \Delta z$ = 0.75 mm × 0.75 mm × 1.5 mm, $N_x \times N_y \times N_z = 512 \times 256 \times 100$, $\theta = 2°$, $N_{acq} = 1$, τ_{RF} = 2.56 msec, G_{ss} = 4.8 mT/m; (b) $\theta = 10°$; (c) $\theta = 20°$.

Incoherent steady-state methods commonly use T_R values which are short enough that natural spoiling does not occur. These implementations use transverse magnetization spoiling mechanisms which require a detailed knowledge of steady-state free precession signal behavior. For the time being, it is assumed that spoiling is achieved prior to each new RF pulse even in the short-T_R case.

Approach to Incoherent Steady-State

Although equilibrium solutions have been found, the general transient behavior of the magnetization is yet to be evaluated. Some tissues will reach a steady-state equilibrium more quickly than others, depending on their T_1 values. The mathematical description of this approach to steady-state is the goal of this subsection. If the steady-state is reached before data acquisition is started, then there will be no filtering effects in the phase encoding direction. Otherwise, the signal changes from cycle to cycle, and the image quality can suffer. This ringing is reminiscent of the filtering effects in the read direction due to T_2 decay. This is described at the end of the discussion in this subsection.

Let us evaluate how many pulses it takes for a tissue magnetization to approach some fraction of its steady-state value. For convenience, the short-hand notation of $M_z^{\pm}(n)$ is used to denote $M_z(nT_R^{\pm})$. From Equation B5.1.10, which required that the transverse magnetization just prior to any RF pulse is zero, the longitudinal magnetization at the end of the $(n-1)^{st}$ repetition period is given by:

$$M_z^-(n) = M_z^-(n-1)\cos\theta E_1 + M_0(1-E_1) \qquad n \geq 1 \qquad \textbf{(B5.1.20)}$$

A first recursion of this equation in terms of $M_z^-(n-2)$ is:

$$M_z^-(n) = M_z^-(n-2)(\cos\theta E_1)^2 + M_0(1-E_1)\cos\theta E_1 + M_0(1-E_1) \qquad n \geq 2 \qquad \textbf{(B5.1.21)}$$

Continuing this iteration yields:

$$\begin{aligned} M_z^-(n,\theta) &= \left[\sum_{l=0}^{n-1}(\cos\theta E_1)^l(1-E_1)M_0\right] + M_0(\cos\theta E_1)^n \qquad n \geq 1 \\ &= M_0(1-E_1)\frac{\left(1-(\cos\theta E_1)^n\right)}{1-\cos\theta E_1} + M_0(\cos\theta E_1)^n \qquad n \geq 1 \end{aligned} \qquad \textbf{(B5.1.22)}$$

This expression is most easily evaluated at $\theta = \theta_E$. Using $\cos\theta_E = E_1$ from Equation B5.1.18, Equation B5.1.22 becomes:

$$M_z^-(n,\theta_E) = M_0\frac{\left(1-E_1^{2n}\right)}{1+E_1} + M_0E_1^{2n} \qquad n \geq 1 \qquad \textbf{(B5.1.23)}$$

In the new notation, the steady-state value is:

$$\lim_{n\to\infty} M_z^-(n,\theta_E) = M_{ze}(\theta_E) = M_0/(1+E_1) \qquad \textbf{(B5.1.24)}$$

The relative error in estimating $M_z^-(n)$ by $M_z^-(\infty)$ at the $(n+1)^{st}$ pulse for the Ernst angle is given by:

$$\alpha \equiv \frac{M_z^-(n,\theta_E) - M_{ze}(\theta_E)}{M_{ze}(\theta_E)} = E_1^{2n+1} \qquad \textbf{(B5.1.25)}$$

Hence, the number of pulses n_α required to reduce Equation B5.1.25 to a given α is:

$$n_\alpha = \left[-\frac{T_1}{2T_R}\ln\alpha - \frac{1}{2} \right] \qquad \textbf{(B5.1.26)}$$

where the square brackets denote the next largest integer of the argument. For the case when T_R = 40 msec, the approximate values of n_α for α = 0.01 and α = 0.1 for different tissues are tabulated in Table B5.1.2. The T_R = 400 msec case is tabulated in Table B5.1.3. From these tables, note that $n_\alpha T_R$ is roughly a constant for each individual tissue and fixed α, so that once n_α is found for a given T_R, it is easily found for any other T_R.

The situation in the general θ case is described from Equation B5.1.22:

$$\begin{aligned} M_z^-(n,\theta) &= M_{ze}(\theta)\left(1-(E_1\cos\theta)^n\right) + M_0(E_1\cos\theta)^n \\ &= \left(M_0 - M_{ze}(\theta)\right)(E_1\cos\theta)^n + M_{ze}(\theta) \end{aligned} \qquad \textbf{(B5.1.27)}$$

Equation B5.1.27 describes an exponential decay of $M_z^-(n)$ from M_0 to M_{ze} with a rate determined by the quantity $E_1\cos\theta$. This means that the approach to steady state is faster if either E_1 or $\cos\theta$ or their product is small. So, shorter T_1 tissues reach steady-state faster as a function of RF pulse number; similarly, all tissues reach steady-state faster for longer T_R values and as θ increases in the range $0 \le \theta \le 90°$.

The plots for magnetization as a function of pulse number n for θ = 10° are shown for two different T_R values in Figure B5.1.5. This figure demonstrates that the steady-state

Table B5.1.2 Approximate Values of n_α for α = 0.01 and α = 0.1 for Different Tissues (T_R = 40 msec)[a]

	CSF	GM	WM	Fat
α = 0.01	259	55	35	14
α = 0.1	130	26	17	7

[a]The pulse number n_α for two α values and different tissues at their respective Ernst angles at 1.5 T when T_R = 40 msec. See Figure B5.1.5A.

Table B5.1.3 Approximate Values of n_α for α = 0.01 and α = 0.1 for Different Tissues (T_R = 400 msec)[a]

	CSF	GM	WM	Fat
α = 0.01	26	5	3	1
α = 0.1	13	3	2	1

[a]As in Table B5.1.2, but for T_R = 400 msec. See Figure B5.1.5B.

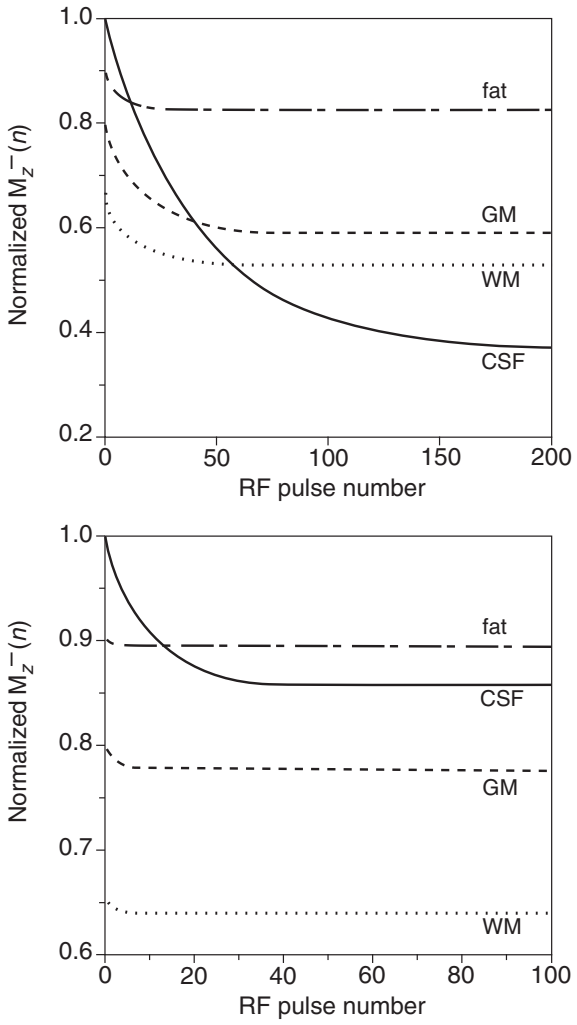

Figure B5.1.5 Plot of $M_z^-(n)$ as a function of RF pulse number n for GM, WM, CSF, and fatty tissue at a common flip angle $\theta = 10°$ for (**A**) $T_R = 40$ msec (**B**) and $T_R = 400$ msec. Note the difference between these data, and Tables B5.1.2 and Table B5.1.3 where the individual Ernst angles are used.

equilibrium longitudinal magnetization is often small compared to the thermal equilibrium value of M_0.

Even though $M_{ze}(\theta_E)$ from tissues with long T_1 values may be small, it is possible to get a rather large signal during the smaller n, presteady-state cycles, despite the filtering effect. For example, CSF could appear falsely bright in a T_1-weighted image ($\theta > \theta_E$) if n_α for CSF is greater than the number of phase encoding lines in a 2-D scan. Note the small RF pulse number regime in Figures B5.1.5A and B5.1.5B where the CSF signal is much greater than its equilibrium value. To obtain the expected contrast, the transverse magnetization must reach steady-state before the imaging experiment is carried out. Only after n_α cycles, for $\alpha << 1$, can true T_1-weighted data be obtained without filtering effects. This can significantly lengthen the imaging time for a short-T_R 2-D scan, but it is less of a problem in a short-T_R 3-D scan.

If the *k*-space data are collected sequentially from $-k_{PE}$ to $+k_{PE}$, a relatively large transient signal does not affect the image very much since the filtering occurs only at high *k*-space values where the absolute signal is small. In fact, this high-pass filtering enhances the edge information on the image and could be quite advantageous. Further, by the time the origin of *k*-space is reached, the signal will generally have reached steady-state and the image contrast is not reversed as in the case briefly discussed in the previous paragraph.

Generating a Constant Transverse Magnetization

Maximizing signal for a fixed T_R by choosing a specific flip angle (the Ernst angle) is important in fast imaging; however, this may not be the most efficient method to obtain high signal if only a limited number of RF pulses are employed to complete the entire imaging experiment.

For short-T_R 2-D scans, it is possible to eliminate the filtering effect caused by the variations in magnetization at each new RF pulse during the approach to steady-state equilibrium. Suppose that the transverse magnetization excited by each RF pulse is forced to be equal to that created by the previous RF pulse. That is, the second pulse is designed to return the transverse magnetization to $M_0 \sin\theta_1$, its value after the first pulse and so on. By making:

$$M_{\perp}^{+}(n,\theta_{n+1}) = M_{\perp}^{+}(n-1,\theta_n) \qquad \textbf{(B5.1.28)}$$

for any *n*, the filtering effect can be successfully eliminated and the transverse magnetization kept constant. Equivalently, the flip angle θ_n is modified from one pulse to the next such that the longitudinal magnetization $M_z^-(n-1, \theta_n)$ satisfies the condition:

$$M_z^-(n)\sin\theta_{n+1} = M_z^-(n-1)\sin\theta_n \qquad \textbf{(B5.1.29)}$$

This works as long as Equation B5.1.29 does not require θ_{n+1} to be larger than $\pi/2$. This results from the fact that if the longitudinal magnetization recovered in a given cycle is less than the desired transverse magnetization, even the maximum rotation of $\pi/2$ is insufficient to recover the correct transverse magnetization. As a result, $\theta_n = \pi/2$ is often used as the terminating condition for this method of producing constant magnetization.

The method of changing the flip angle as a function of RF pulse number is typically used in extremely short-T_R 2-D SSI imaging applications. A predetermined terminal flip angle is required to occur after a target number of RF pulses *p*. There is no analytic closed form for θ_n as a function of *n*. The values for $\{\theta_n\}$ are evaluated numerically; the results of one such simulation are shown in Figure B5.1.6.

It is possible to make some general remarks concerning the behavior of θ_n in the above method. Once the spin system is disturbed by the first RF pulse, there is less longitudinal magnetization available for the following RF pulses since T_R is extremely short (see Fig. B5.1.5). The flip angle must therefore increase with RF pulse number to create a constant transverse magnetization. If θ_1 is too small, the longitudinal magnetization is barely disturbed and almost full magnetization is available for the next pulse(s), and θ_n increases very slowly with *n*. If the terminal flip angle is 90°, as it is in most 2-D imaging applications, this target is reached only after a very large number of pulses. If it is desired that the total number of pulses not be too large, then the value of θ_1 should not be too small. The increase in flip angle with *n*, which is slow if θ_1 is small and accelerates as θ_n increases, is apparent in Figure B5.1.6. The figure shows the case where *p* is chosen to be 30, corresponding to $\theta_1 \sim 13°$ for a tissue with T_1 = 950 msec and T_R = 10 msec.

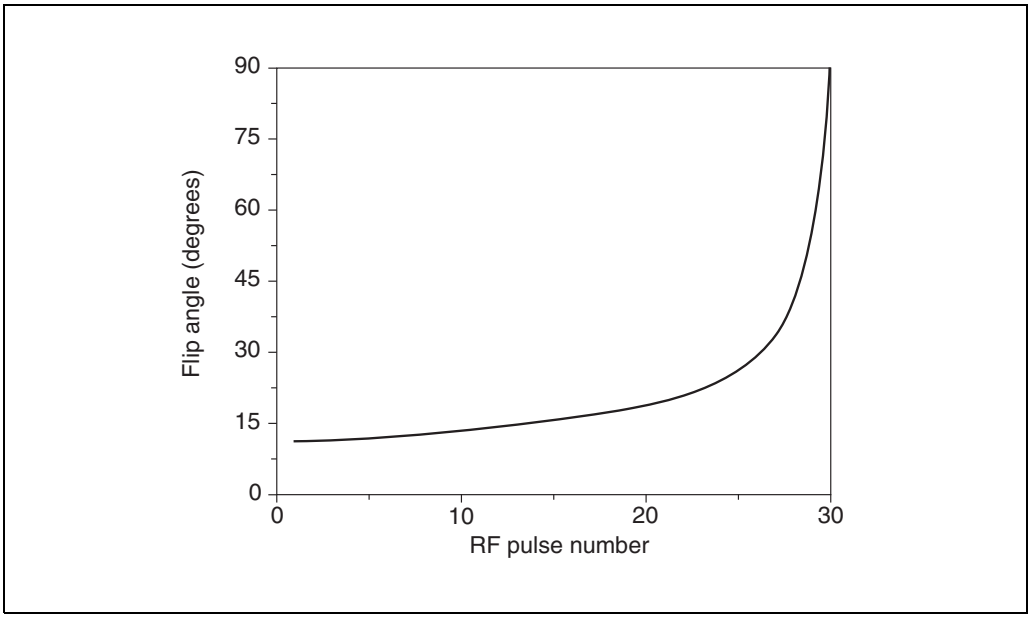

Figure B5.1.6 Use of a variable flip angle which increases as a function of RF pulse number in order to force a constant transverse magnetization from one RF pulse to the next. The plot was obtained for a terminal pulse number $p = 30$, with $T_1 = 950$ msec and $T_R = 10$ msec.

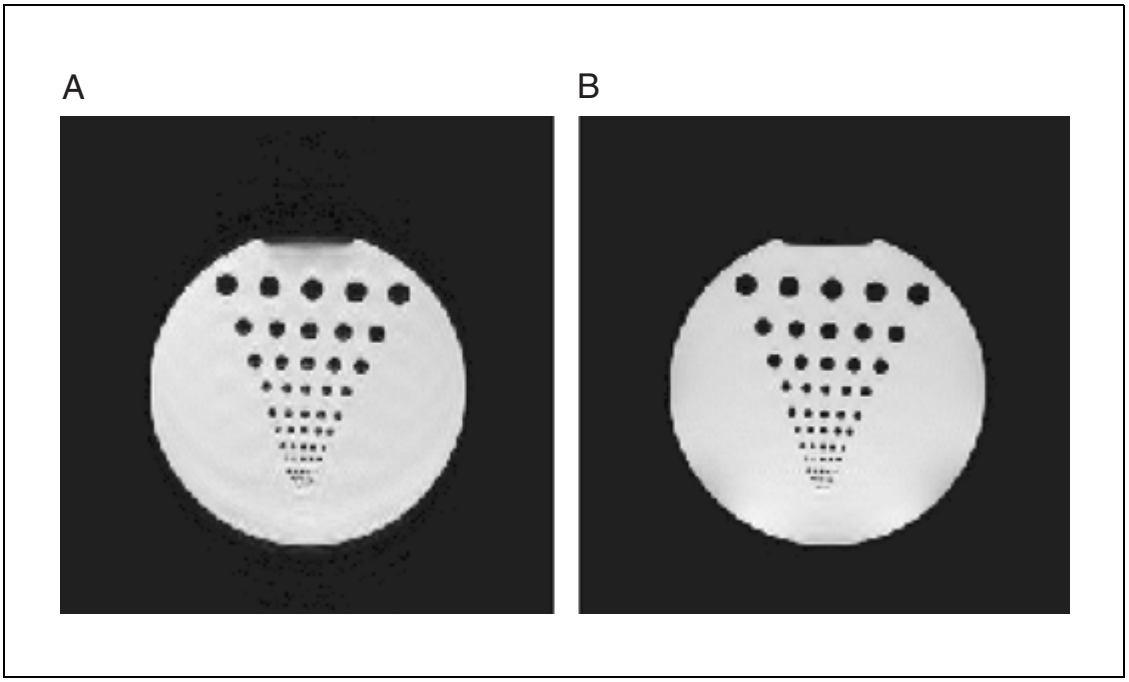

Figure B5.1.7 A comparison of the use of variable versus fixed flip angle in short-T_R 2-D imaging. (**A**) An image obtained with fixed flip angle has more ringing in the phase encoding direction than (**B**) an image obtained according to the method described in the text. The ringing occurs in (A) due to the fact that the signal varies with RF pulse number before steady-state has been achieved. Imaging parameters: (A) T_R/T_E = 1500 msec/7.3 msec, $T_s = 7.68$ msec, $\Delta x \times \Delta y \times \Delta z = 1.17$ mm $\times$ 1.17 mm $\times$ 5.0 mm, $N_x \times N_y = 256 \times 256$, $\theta = 90°$, $N_{acq} = 1$, $\tau_{RF} = 1.024$ msec, $G_{ss} = 11.0$ mT/m; (B) θ = variable (last flip angle (ninth flip angle in this case) is 90°).

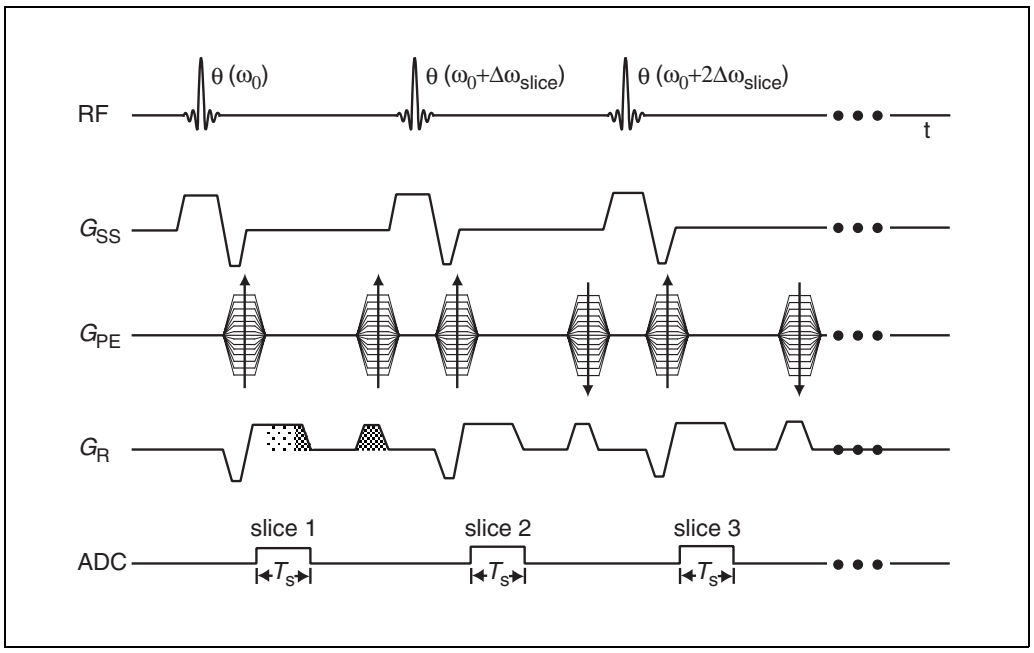

Figure B5.1.8 A multislice gradient echo sequence.

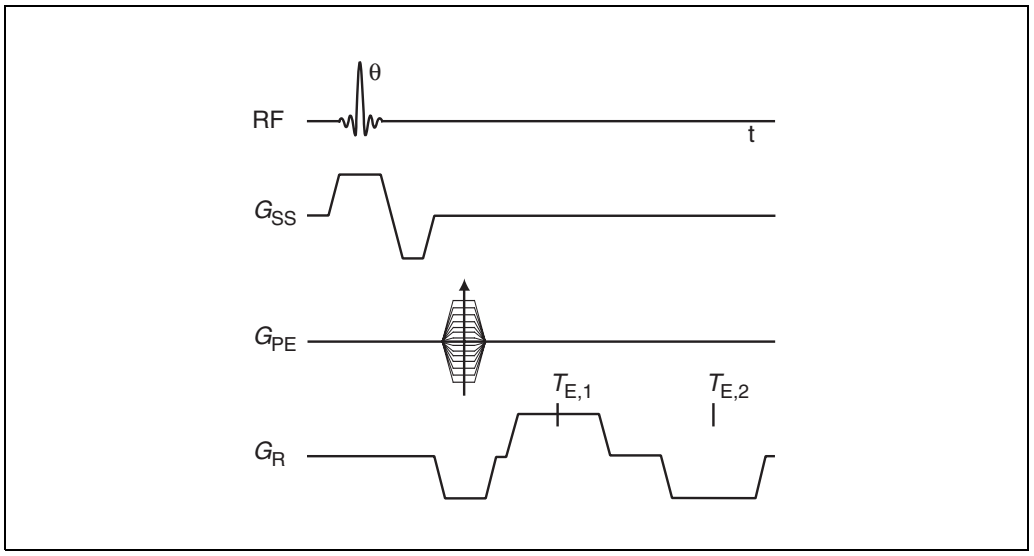

Figure B5.1.9 The read and phase encoding gradient waveforms with an arbitrary flip angle θ for a simple double echo gradient echo sequence.

The advantage of forcing steady-state using variable flip angles is illustrated in Figure B5.1.7. An image obtained with fixed flip angle is compared to an image obtained with a flip angle varied to excite constant magnetization at each new RF pulse. The former exhibits more ringing and some ghosting in the phase encoding direction. As discussed before, the ringing in the fixed flip angle case (Fig. B5.1.7A) is a result of the exponential approach to steady-state as a function of RF pulse number of the excited magnetization, which is then phase encoded. The ghosting is a result of some periodic amplitude inconsistencies created along the phase encoding direction.

Multislice Gradient Echo and Double Echo Gradient Echo Sequences

The simplest way to collect multislice images is to use a 3-D sequence. The difference between a 2-D sequence (Fig. B5.1.1) and a 3-D sequence is that a 3-D sequence has partition encoding tables along the slice select direction. These tables are the same as those phase encoding tables in the phase encoding direction.

On the other hand, we could use a multislice 2-D sequence to collect multislice images. A sequence diagram for multislice imaging is shown in Figure B5.1.8. The first RF pulse and the slice select gradient excites slice 1. The second RF pulse and the second slice select gradient excites slice 2 by applying a resonance frequency different from the resonance frequency of the first RF pulse. In each slice, only one line in *k*-space has been sampled. The sequence repeats itself after many slices have been excited and sampled for a given phase encoding line. This means the repetition time T_R of each individual slice is long and the advantage of a long T_R is that the MR signal can be higher than the signal obtained from a short T_R 3-D scan (due to the regrowth of the longitudinal magnetization).

Another possible structure of a gradient echo sequence is a multiple echo gradient echo sequence. Figure B5.1.9 shows a simple double gradient echo sequence. For a multiple echo gradient echo sequence, the reader can imagine that the read gradients based on Figure B5.1.9 oscillate with different polarities. (For example, the gradient lobe with the third gradient echo will have the same polarity as the gradient lobe with the first gradient echo, $T_{E,1}$.)

KEY REFERENCES

Bydder, G.M. and Young, I.R. 1985. Clinical use of the partial and saturation recoverey sequences in MR imaging. *J. Comput. Assist. Tomogr.* 9:1020.

This paper proposed different short T_E, fast imaging methods.

Ernst, R.R. and Anderson, W.A. 1966. Application of Fourier transform spectroscopy to magnetic resonance. *Rev. Sci. Instrum.* 37:93.

This article covers both the coherent and incoherent steady-states and gives expressions for flip angles which maximize the signal (hence the name "Ernst angle").

Haacke, E.M., Weilopolski, P.A., and Tkach, J.A. 1991. A comprehensive technical review of short T_R, fast magnetic resonance imaging techniques. *Rev. Magn. Reson. Med.* 3:53.

This article gives a modern review of the steady-state, fast imaging methods.

Haacke, E.M., Brown, R.W., Thompson, M.R., and Venkatesan, R. 1999. Magnetic Resonance Imaging: Physical Principles and Sequence Design. John Wiley & Sons, New York.

This text covers the technical aspects presented here, but in more detail, and also discusses more advanced materials.

Haase, A., Frahm, J., Matthei, D., Hannicke, W., and Merboldt, K.-D. 1986. FLASH imaging: Rapid imaging using low flip angle pulses. *J. Magn. Reson.* 67:256.

This article proposed different short T_E, fast imaging methods.

Hennig, J. 1991. Echoes—how to generate, recognize, use or avoid them in MR imaging sequences. Part I: Fundamental and not so fundamental properties of spin echoes. *Concepts Magn. Reson.* 3:125.

This text gives a modern review of the steady-state, fast imaging methods.

Hennig, J. 1991. Part II: Echoes in imaging sequences. *Concepts Magn. Reson.* 3:179.

This paper gives a modern review of the steady-state, fast imaging methods.

Oppelt, A., Graumann, R., Barfuss, H., Fischer, H., Hertl, W., and Schajor, W. 1986. FISP: A new fast MRI sequence. *Electromedica* 3:15.

This paper proposed different short T_E, fast imaging methods.

van der Muelen, P., Croen, J.P., and Cuppen, J.J.M. 1985. Very fast MR imaging by field echoes and small angle excitation. *Magn. Reson. Imaging* 3:297.

This article proposed different short T_E, fast imaging methods.

Zur, Y., Wood, M.L., and Neuringer, L.J. 1991. Spoiling of transverse magnetization in steady-state sequences. *Magn. Reson. Med.* 21:251.

A specific solution to the RF spoiling problem is given in this article.

Contributed by Yu-Chung Norman Cheng and E. Mark Haacke
Case Western Reserve University
Cleveland, Ohio and
The MRI Institute for Biomedical Research
St. Louis, Missouri